Research article

Atrophy of hippocampal subfields and amygdala nuclei in subjects with mild cognitive impairment progressing to Alzheimer's disease

Miriam Punzi [a,d], Carlo Sestieri [a,b], Eleonora Picerni [a], Antonio Maria Chiarelli [a], Caterina Padulo [a,c], Andrea Delli Pizzi [a], Maria Giulia Tullo [a], Annalisa Tosoni [a], Alberto Granzotto [a,d], Stefania Della Penna [a,b], Marco Onofrj [a], Antonio Ferretti [a,b,e], Stefano Delli Pizzi [a,b,d,*], Stefano L. Sensi [a,b,d,**], for the Alzheimer's Disease Neuroimaging Initiative[1]

[a] Department of Neuroscience, Imaging, and Clinical Sciences, University "G. D'Annunzio of Chieti-Pescara", Chieti, 66100, Italy
[b] Institute for Advanced Biomedical Technologies (ITAB), "G. D'Annunzio of Chieti-Pescara", Chieti, 66100, Italy
[c] Department of Humanities, University of Naples Federico II, Naples, 80133, Italy
[d] Molecular Neurology Unit, Center for Advanced Studies and Technology (CAST), University "G. D'Annunzio of Chieti-Pescara", Chieti, 66100, Italy
[e] UdA-TechLab, Research Center, University "G. D'Annunzio" of Chieti-Pescara, 66100, Chieti, Italy

ARTICLE INFO

ABSTRACT

The hippocampus and amygdala are the first brain regions to show early signs of Alzheimer's Disease (AD) pathology. AD is preceded by a prodromal stage known as Mild Cognitive Impairment (MCI), a crucial crossroad in the clinical progression of the disease. The topographical development of AD has been the subject of extended investigation. However, it is still largely unknown how the transition from MCI to AD affects specific hippocampal and amygdala subregions. The present study is set to answer that question. We analyzed data from 223 subjects: 75 healthy controls, 52 individuals with MCI, and 96 AD patients obtained from the ADNI. The MCI group was further divided into two subgroups depending on whether individuals in the 48 months following the diagnosis either remained stable (N = 21) or progressed to AD (N = 31). A MANCOVA test evaluated group differences in the volume of distinct amygdala and hippocampal subregions obtained from magnetic resonance images. Subsequently, a stepwise linear discriminant analysis (LDA) determined which combination of magnetic resonance imaging parameters was most effective in predicting the conversion from MCI to AD. The predictive performance was assessed through a Receiver Operating Characteristic analysis. AD patients displayed widespread

subregional atrophy. MCI individuals who progressed to AD showed selective atrophy of the hippocampal subiculum and tail compared to stable MCI individuals, who were undistinguishable from healthy controls. Converter MCI showed atrophy of the amygdala's accessory basal, central, and cortical nuclei. The LDA identified the hippocampal subiculum and the amygdala's lateral and accessory basal nuclei as significant predictors of MCI conversion to AD. The analysis returned a sensitivity value of 0.78 and a specificity value of 0.62. These findings highlight the importance of targeted assessments of distinct amygdala and hippocampus subregions to help dissect the clinical and pathophysiological development of the MCI to AD transition.

1. Introduction

Alzheimer's disease (AD) is one of the most common forms of age-related neurodegenerative dementia. It is characterized by a progressive deterioration of cognitive abilities and severe behavior changes [1]. AD is preceded by a prodromal stage known as Mild Cognitive Impairment (MCI), a crucial crossroad in clinical progression. A fraction of MCI people (10–15%) progress to AD each year, compared to 1–2% of the healthy older population [2]. Since the neurodegenerative process leading to AD begins over a decade before a clinical diagnosis can be made [3], the early identification of the brain modifications associated with MCI is critical to catching AD at its initial stage and establishing timely therapeutic interventions.

Magnetic Resonance Imaging (MRI) is a valuable, non-invasive tool for studying the macrostructural changes characterizing the AD spectrum [4–11; Table 1]. Neuroimaging research has primarily focused on medial temporal structures, such as the hippocampus [12–18] and, more recently, the amygdala [19–21]. These regions are of particular interest as they exhibit early signs of tau pathology, a process strongly associated with neurodegeneration and cognitive decline in AD [19,20,22–27]. A recent MRI study has shown that the extent of atrophy in the amygdala and the hippocampus is associated with the progression from MCI to AD [21].

However, a potential limitation of previous studies is that they have considered the hippocampus and the amygdala as a whole, thereby neglecting these regions' anatomical and functional heterogeneity. The hippocampus and the amygdala are complex structures composed of multiple subregions, each with distinct connections and functions [28]. Understanding this anatomical and functional diversity is crucial, given the differential vulnerability to age-related neurodegenerative disorders [29–31]. While previous evidence revealed a hierarchical accumulation of AD-related neuropathology across specific amygdala [32] and hippocampal subregions [33], MRI studies investigating the macro-structural damage in MCI at a finer subregion scale have yielded conflicting results [9,11,12,21,34–40]. This apparent inconsistency can be explained by the small sample size of the cohorts under examination [12,35, 36], the lack of clinical follow-up to differentiate converters and non-converters [34–36,39,40], and the analysis methods based on manual or semiautomatic procedures including the investigation of a limited number of subregions [11,12,21,38].

In the current study, we addressed these issues by applying a probabilistic method that combines individual morphometric measures with a-priori information from ex-vivo MRI and histology [28,41]. Specifically, we investigated whether analysis of the pattern of grey matter (GM) atrophy in specific hippocampal and amygdala subregions allows us to differentiate between MCI subjects converting to AD (c-MCI) and MCI subjects who remained clinically stable (s-MCI). Considering that the basal and cortical nuclei of the

Table 1

A comparative table of Machine Learning studies investigating structural changes in hippocampal or amygdala's subregions in progressive MCI subjects.

Reference	Kwak (7)	Guo (8)	Izzo (9)	Vasta (10)	Khan (11)
Data source	ADNI-2/GO (MRI 3T)	ADNI1 (MRI 1.5T)	ADNI1 (MRI 1.5T)	ADNI-1 (MRI 1.5T) ADNI-2 (MRI 3T)	Add Neuro Med Cons.+ ADNI 1 (MRI 1.5T)
Sample size of *p*-MCI/s-MCI	118/263	111/102	60/509	32/89	90/357
Clinical follow-up	18 months	24 months	60 months	18 months	12 months
Significative hippocampal subfields	Presubiculum CA1 Subiculum Molecular layer	CA2-3 Subiculum CA4-DG Presubiculum	Fissure Subiculum Presubiculum	Subiculum Presubiculum	Presubiculum
Significative amygdala's nuclei	NA	NA	NA	NA	NA
Method	Deep convolutional neural network (accuracy of 75.9%)	SVM-RFE (accuracy of 76.9%)	LVQ (accuracy of 75%)	SVM (accuracy of 71%) + NBC (accuracy of 68%) + NNC (accuracy of 72%)	MRI and multivariate OPLS technique (accuracy 81.1%)
Segmentation Tool	FS v.6.0 (12 subfields)	FS v. 5.3 (8 subfields)	FS v. 6.0 (12 subfields)	FS v. 5.0 (7 subfields)	FS v. 5.1 (7 subfields)

Abbreviations: ADNI=Alzheimer's Disease Neuroimaging Initiative; CA=Cornu Ammonis; DG = Dentate Gyrus; FS= FreeSurfer; LVQ = Learning Vector Quantization; NA = not available; NBC=Naïve Bayesian Classifier; NNC=Neural Networks Classifier; *p*-MCI = progressive Mild Cognitive Impairment subjects; s-MCI = stable Mild Cognitive Impairment subjects; MRI = Magnetic Resonance Imaging; RFE=Recursive Feature Elimination; SVM= Support Vector Machine.

amygdala, and the Cornu Ammonis (CA) −1 and subiculum areas of the hippocampal formation, are the most affected regions by AD pathology [32,33], we predicted that higher/selective atrophy in these regions would be associated with conversion to AD. To further examine the spatial specificity of the results, we included structural measurements of the thalamus and the basal ganglia, brain areas also commonly targeted by AD pathology [42,43]. Identifying atrophic nuclei of additional brain regions provides valuable insights into the underlying pathophysiological processes related to the clinical progression to AD of MCI subjects.

2. Material and methods

2.1. Study data, inclusion, and diagnostic criteria

All the data used for this article were obtained from the Alzheimer's Disease Neuroimaging Initiative (ADNI-3) database, a multisite study, including 59 research centers in the United States and Canada. ADNI-3 was launched in late 2016 as a public/private partnership to determine the relationships among the clinical, neuropsychological, imaging [MRI, Positron Emission Tomography (PET)], genetic, and biochemical biomarker characteristics of the entire spectrum of sporadic late-onset AD. For updated information on the initiative, see ADNI website (http://adni.loni.usc.edu). The study was performed according to ethical standards and the Declaration of Helsinki (2000). Informed consent was obtained from study participants or legally authorized representatives. Subjects enrolled had a good general health status, and no diseases were expected to interfere with the study. Details on the study protocol are reported on the ADNI website (http://www.adni-info.org).

Two hundred twenty-three subjects were included in this study, divided into 75 HC, 52 patients with MCI, and 96 patients with probable AD. The HC group included cognitively normal individuals who did not convert to MCI or dementia (criteria for the HC group established both at baseline and in the follow-up at 48 months). Out of the 52 participants meeting the criteria for MCI, 59.6% (n = 31) converted to an AD diagnosis (c-MCI) within 48 months of clinical follow-up. The MCI subjects who did not convert to AD (n = 21) within 48 months of clinical follow-up were defined as s-MCI.

T1-weighted images were acquired by a 3T scanner using a harmonized protocol and identical acquisition parameters to minimize site differences (https://adni.loni.usc.edu/methods/mri-tool/mri-analysis/). Our study included only the subjects who had completed baseline 3D T1-weighted scans and neuropsychological/clinical investigations. Subjects who underwent a scanning session but displayed incomplete clinical and demographic information and/or explained technical issues in their MRI raw data (severe motion, missing volumes, or corrupted files) were excluded from the study sample (Supplementary Fig. 1).

2.2. Clinical assessments

At the time of the MRI scan, all participants were extensively evaluated on the following set of clinical and neuropsychological assessments: 1) the Mini Mental State Examination (MMSE) and the Montreal Cognitive Assessment (MoCA) to investigate global cognition; 2) the Functional Activities Questionnaire (FAQ) for the assessment of daily living activities; 3) the Alzheimer's Disease Assessment Scale Cognitive subscales (ADAS-11 items scores; ADAS-13 items scores; ADAS-Q4 delayed word recall subscale) to evaluate the severity of impairments of memory, learning, language, praxis, and orientation; 4) the Clock Drawing Test (CT) to assess dysfunction of visuo-constructive abilities; 5) the Animal Fluency and the Multilingual Naming Test (MINT) to detect language capacities and naming deficits; 6) the Trail Making Test (time to completion, TMT parts A and B) for processing speed and executive function; 7) the Rey Auditory Verbal Learning Test (RAVLT) to assess auditory verbal learning and memory (immediate memory, learning, delayed recall, and delayed recognition) and the Logical Memory II (LM), subscale of the Wechsler Memory Scales Revised (WMS-R) Story A for immediate and delayed recall; 8) the Neuropsychiatric Inventory (NPI) and the Geriatric Depression Scale (GDS) to characterize and obtain information on psychopathological profile and behavioral disturbances.

The HC subjects included in our study were free of significant impairment in cognitive functions or daily living activities. They had MMSE scoring between 27 and 30 inclusive, a global score of 0 (in particular, Memory Box score = 0) on the Clinical Dementia Rating Scale (CDR-RS), and normal memory function documented by scoring above education-adjusted cut-offs on the LM (>9 for 16 or more years of education, >5 for 8–15 years of education, >3 for 0–7 years of education).

The inclusion criteria for MCI subjects were MMSE scores between 24 and 30, subjective memory concerns, memory impairments identified by the partner, CDR Memory Box score >0.5, and abnormal memory function documented by scoring below education-adjusted cut-offs on the LM (<11 for 16 or more years of education; ≤9 for 8–15 years of education; ≤6 for 0–7 years of education). The general cognition status and functional performances of MCI were sufficiently preserved to exclude a diagnosis of AD.

AD patients fulfilled the criteria of probable AD in line with the criteria set by the National Institute of Neurologic and Communicative Disorders and Stroke and by the Alzheimer's Disease and Related Disorders Association. Patients with AD reported MMSE scores between 20 and 26 (inclusive). For more details about the ADNI-3 inclusion criteria, see:https://adni.loni.usc.edu/wp-content/uploads/2012/10/ADNI3-Procedures-Manual_v3.0_20170627.pdf

The conversion from MCI to dementia was clinically assessed by skilled ADNI clinicians using information from the patient and a knowledgeable caregiver, biological markers, and neuropsychological assessment.

The apolipoprotein E (APOE) genotyping for participants was performed as previously described [44]. The APOE ε4 status, including individuals with one or more ε4 alleles, was investigated at the screening stage. The data was present for approximately 93.7 % of the total cohort.

2.3. MRI data acquisition and analysis

Standardized MRI data acquisition techniques were in place for ADNI to ensure homogeneity across data acquisition sites. A detailed description of the ADNI data acquisition protocol can be found at https://adni.loni.usc.edu/adni-3/procedure-manuals/. The imaging protocol included a 3T1-weighted sagittal 3D MPRAGE volume (voxel size $1.05 \times 1.05 \times 1.2$ mm^3).

T1-weighted images were processed with FreeSurfer 7.3 using the "recon-all -all" command line. Briefly, this processing includes motion correction and intensity normalization of T1-weighted images, removal of non-brain tissue using a hybrid watershed/surface deformation procedure, automated Talairach transformation, segmentation of the subcortical white matter (WM) and deep GM volumetric structures (including the hippocampus, amygdala, caudate, putamen, ventricles), tessellation of the GM WM matter boundary, and derivation of cortical thickness. The tool provided an automated reconstruction and labeling of cortical and subcortical regions and a measure of estimated Intracranial Volume (ICV). The "segmentHA_T1. sh'' script was subsequently used to compute the parcellation and volume quantification of different hippocampal [41] and amygdala [28] subregions. The hippocampus was segmented into nineteen subfields for each hemisphere (Fig. 1A): the head and body of CA-1/3/4, the head and body of presubiculum and subiculum, the head and body of Granule Cell (GC) - Molecular Layer (ML) - dentate gyrus (DG), molecular layer, as well as the parasubiculum, the hippocampal tail, the hippocampal fissure, the fimbria, and the hippocampal amygdala transition area (HATA). Of note, the CA2 field was included in the CA3 field. The amygdala was segmented into 9 nuclei for each hemisphere (Fig. 1B): the accessory basal nucleus, the anterior amygdaloid area (AAA), the basal nucleus, the central nucleus, the cortical-amygdaloid transition area, the cortical nucleus, the medial nucleus, the lateral nucleus, and the para-laminar nucleus. The volume of each subregion was normalized (divided) by the estimated intracranial volumes (eTIV). We thoroughly examined all the hippocampal subfields and amygdala nuclei segmentations and found no issues in sub-regional parcellation. No additional manual corrections were made, as the anatomical boundaries consistently matched the atlas and remained uniform across subjects, a result confirmed by meticulous visual inspection.

2.4. Statistical analysis

Analysis of variance and Bonferroni post hoc tests were used to evaluate group differences regarding demographic, neuropsychological, and clinical data. The categorical variables were analyzed using chi-square tests. For the MRI measures, a MANCOVA (diagnosis: 4 levels [HC, s-MCI, c-MCI, AD]; sex), followed by Turkey's post-hoc comparison, was applied to test the differences among groups. Age and education level were added to the model to control for their potential confounding effect.

All MRI volumes of the hippocampus/amygdala subregions were additionally included in a stepwise linear discriminant analysis (LDA) to determine whether a set of variables effectively predicted category membership (s-MCI or c-MCI) and to what extent. The
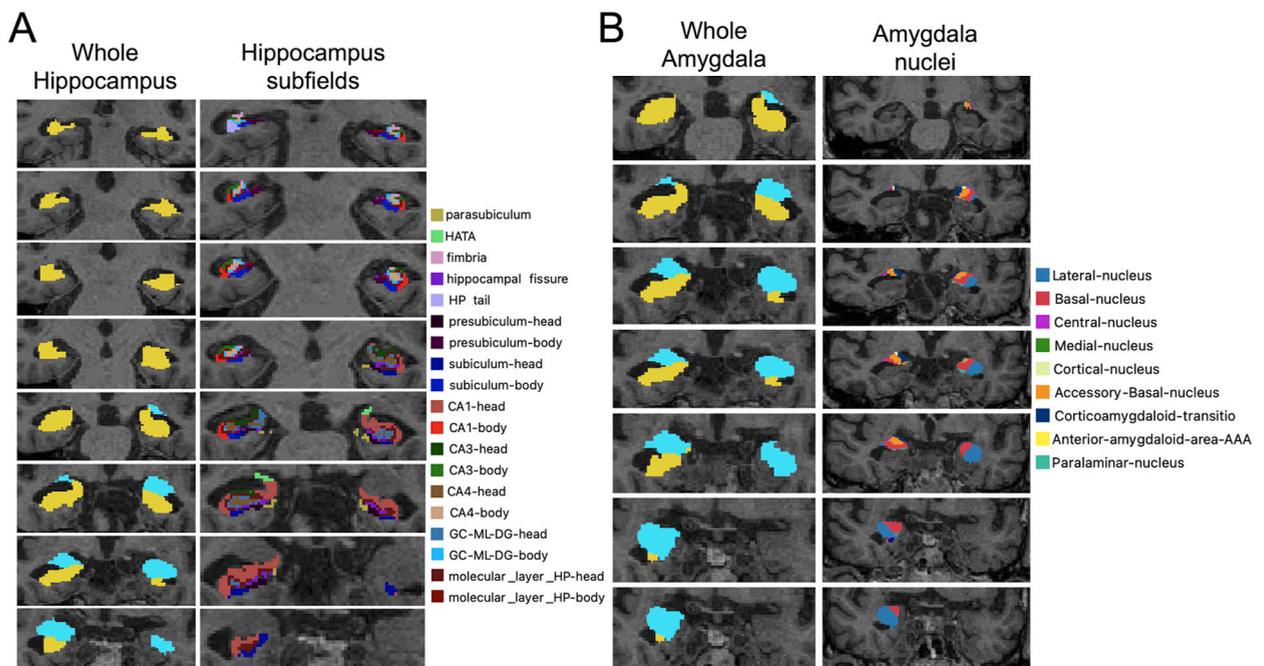
Fig. 1. Representative images show the MRI segmentation of the amygdala, hippocampus, and their subregions. (A) The segmented whole left and right structures of the hippocampus are depicted in yellow, and their parcellation into specific subfields. (B) The segmented whole left and right sub-structures of the amygdala are depicted in light blue, and their parcellation into 9 nuclei. The images are presented in the neuroradiological convention.

stepwise LDA selected the optimal number of features by iteratively adding one variable to the prediction to try and maximize the Area under the Curve (AUC) of the classification until an extra-sum-of-squares F test was not significant. The generalization of the model was assessed using a leave-one-out cross-validation (CV) approach. In this approach, the model is trained on all data except one subject in an iterative manner. The out-of-sample performance (i.e., generalization) is assessed on the removed subjects by combining all iterations. For each interaction, a set of selected variables and their respective coefficients were determined, indicating the unique contribution of each variable to the predictive function. Finally, a Receiver Operating Characteristic (ROC) analysis was used on the out-of-sample prediction to determine an AUC and a cut-off with relative sensitivity and specificity. The analysis investigated whether the volumes of specific subregions could discriminate MCI subjects that would progress to AD. The ROC analysis allows for a comprehensive evaluation of classification performance by assessing the trade-off between true positive rates (sensitivity) and false positive rates (1-specificity).

All statistical tests were two-tailed, and the significant p-value threshold was set at 0.05. All post-hoc comparisons reported in the table are corrected for multiple comparisons.

Within the c-MCI group, Spearman's correlation was employed to examine the association between MRI volumes (which exhibited a significant difference between the s-MCI and c-MCI groups) and the longitudinal variation of neuropsychological/clinical test scores (48 months – baseline score). Bonferroni's correction (6 structures x 24 test) was applied.

Table 2
Demographic, neuropsychological, and clinical features of study groups.

Variable	HC (n = 75)		s-MCI		c-MCI		AD		Group comparison		
									χ^2	P	
N (% male)	75 (47%)		21 (48%)		31 (58%)		96 (57%)		0.758	0.384	
									ANOVA		s-MCI vs.
	Mean	SD	Mean	SD	Mean	SD	Mean	SD	$F_{3.193}$	p	c-MCI
AGE	74.8	6.3	76.7	5.8	74.9	7.9	76.6	8.8	0.137	0.938	NA
Education (y)	17.3	2.3	16.9	3.3	16.3	2.5	15.4	2.5	2.390	0.076	NA
CDR-RS	0.0	0.0	1.4	1.2	2.2	1.1	4.8	2.2	69.637	**<0.001**	0.445
ADAS-11	5.1	2.6	8.7	4.3	12.5	4.3	20.0	7.3	33.947	**<0.001**	0.844
ADAS-13	7.7	4.0	13.2	6.4	20.7	5.8	30.6	8.9	51.958	**<0.001**	0.343
ADAS-Q4	2.3	1.7	3.9	2.3	7.2	2.1	8.7	1.6	74.933	**<0.001**	**0.004**
MMSE	29.4	0.8	28.7	1.8	26.3	2.4	22.6	3.8	48.075	**<0.001**	0.381
MoCA	26.9	2.4	23.4	4.1	21.3	3.3	16.8	4.6	34.903	**<0.001**	0.199
FAQ	0.2	0.7	2.5	3.0	6.3	4.5	15.1	7.5	59.075	**<0.001**	0.098
RAVLT-DR	48.7	11.0	39.5	12.2	27.7	7.9	23.6	7.2	49.521	**<0.001**	0.654
RAVLT-IR	5.5	2.5	5.3	3.1	2.8	2.0	2.0	1.8	35.525	**<0.001**	1.000
RAVLT-L	9.0	4.2	5.8	4.5	1.5	1.9	0.5	1.5	9.773	**<0.001**	0.383
RAVLT-RN	13.8	1.9	12.5	2.8	9.0	3.9	6.5	4.3	57.772	**<0.001**	0.365
RAVLT-T	13.1	2.5	11.3	3.1	6.5	4.3	3.8	3.7	28.531	**<0.001**	0.109
LM-IR	15.7	3.2	12.4	5.0	7.6	3.8	4.7	3.4	50.402	**<0.001**	**0.024**
LM-DR	14.7	3.5	11.0	5.0	4.4	3.5	1.8	2.7	96.380	**<0.001**	**<0.001**
CT-Drawing	4.8	0.5	4.2	1.0	4.3	0.7	3.4	1.5	5.965	**0.001**	1.000
CT-Copy	4.8	0.5	4.6	0.6	4.6	0.7	3.9	1.5	2.012	0.120	NA
TMT-A	29.4	7.9	33.2	15.4	43.7	21.4	62.7	38.3	4.801	**0.004**	0.455
TMT-B	64.9	26.8	94.7	54.9	128.7	53.0	186.4	94.8	17.254	**<0.001**	0.691
AF	22.7	4.9	18.3	5.2	15.7	4.4	12.3	5.1	19.080	**<0.001**	0.109
MINT-SEM	0.3	0.7	0.4	0.9	0.5	0.9	1.0	3.3	1.262	0.294	NA
MINT-UNC	30.5	3.9	27.8	7.2	28.1	4.3	24.7	7.7	7.179	**<0.001**	0.723
MINT-T	30.7	1.9	28.9	4.0	27.6	4.4	25.2	5.8	4.417	**0.007**	0.397
NPI-T	1.2	2.7	2.4	3.5	3.8	4.8	10.2	11.0	6.841	**<0.001**	0.973
GDS	0.7	1.1	2.0	1.9	1.8	1.8	2.2	1.8	6.671	**<0.001**	0.753

Values are expressed as the mean ± standard deviation (SD). Bold values are statistically significant comparisons.
Abbreviations: AD = Alzheimer's disease; ADAS=Alzheimer's Disease Assessment Scale (11 items and 13 items versions); ADAS-Q4 = ADAS delayed word recall subscale; AF = Animal Fluency; CDR-RS=Clinical Dementia Rating Scale; CT-Copy = Clock Test- Copy score; CT- Drawing = Clock Test-Drawing total score; c-MCI = patients with MCI who convert to AD within 48-month follow-up; FAQ=Functional Activities Questionnaire; GDS=Geriatric Depression Scale; HC = healthy control stable after 48 months of follow-up; LM-IR = Logical Memory-Immediate Recall Total Number of Story Units Recalled; LM-DR = Logical Memory-30 min Delayed Recall Total Number of Story Units Recalled; MINT-SEM = Multilingual Naming Test Total Correct - with Semantic Cue; MINT-T = Multilingual Naming Test Total Correct (Uncued + Correct with Semantic cue); MINT-UNC = Multilingual Naming Test Total Uncued Correct; MMSE = Mini-Mental State Examination Total Score; MoCA=Montreal Cognitive Assessment; NA=Not applicable; NPI=Neuropsychiatric Inventory Questionnaire; RAVLT-IR=Rey's Auditory Verbal Learning Test, Immediate Recall (sum of 5 trials); RAVLT-L = Rey's Auditory Verbal Learning Test, learning (trial 5 - trial 1); RAVLT-DR=Rey's Auditory Verbal Learning Test, 30 min Delayed Recall; RAVLT-RN=Rey's Auditory Verbal Learning Test Delayed Recognition; RAVLT-T = Rey Auditory Verbal Learning Test (Trials 1–6); s-MCI = MCI patients who did not convert to AD after 48-month follow-up; TMT = Trail Making Test (parts A and B); y = years.

3. Results

3.1. Demographic, clinical, and cognitive features of the study groups

Summary statistics on demographics are shown in Table 2 and Supplementary Tables 1–4. There was no significant difference in age, sex, and educational levels across study groups (HC, s-MCI, c-MCI, and AD). The positivity for APOE ε4 status was 23% and 28% for the HC and s-MCI, respectively. The AD (62%) and c-MCI (57%) groups had a higher proportion of positivity for APOE ε4 status than the s-MCI and HC groups.

The behavioral analysis at baseline (Table 2) revealed that the s-MCI and the c-MCI groups, although indistinguishable at the clinical examination, differed in terms of immediate and delayed verbal memory (i.e., ADAS-Q4, LM-Immediate Recall, and LM-Delayed Recall). Compared to HC subjects, the MCI subsets, and the AD group exhibited significant impairments in general cognition and memory functions and higher scores on the GDS. However, the AD group showed the most severe deficits across multiple cognitive domains compared to HC and s-MCI subjects. Additionally, the AD patients exhibited more pronounced neuropsychiatric disturbances, as indicated by higher NPI total scores, than the MCI groups (Supplementary Table 1).

We further examined longitudinal variations (difference between the scores at 48 months and baseline) in the neuropsychological scores across the HC and MCI groups (Supplementary Tables 4–5). As reported in Supplemetary Table 4, the c-MCI group exhibited greater variations in global cognition measures compared to the s-MCI group, as indicated by the ADAS-11/13, MOCA, and FAQ. Additionally, in the c-MCI group, there was a significant variation in visuospatial abilities (i.e., CT-Drawing), and neuropsychiatric symptoms (i.e., NPI total). The c-MCI, but not the s-MCI group, showed significant changes in test scores of semantic fluency (i.e., Animal Fluency), executive functions (i.e., TMT-B), and verbal memory (i.e., LM-Immediate Recall).

3.2. MRI volumetry of whole subcortical structures

As shown in Table 3 and Supplementary Table 6, the MANCOVA revealed significant and diffuse atrophy in subcortical structures across different groups, regardless of gender and educational levels. The subcortical structures that exhibited atrophy throughout the AD spectrum included the amygdala, hippocampus, nucleus accumbens, putamen, and thalamus. Compared to s-MCI, c-MCI individuals showed atrophy of the whole hippocampus, while no significant differences were found in the rest of the subcortical regions considered in the present study. Compared with HC subjects, AD and c-MCI subjects exhibited diffuse atrophy of subcortical structures, including the amygdala, hippocampus, putamen, and thalamus. No difference in subcortical volumes was found by comparing the s-MCI and HC groups (Supplementary Table 6).

3.3. MRI volumetry of hippocampal and amygdala subregions

The results of the MANCOVA analysis indicated that, compared to HC subjects, c-MCI individuals, and AD patients, but not the s-MCI group, show diffuse atrophy across all the hippocampal (Table 4; Supplementary Table 7) and amygdala subregions (Table 5; Supplementary Table 9) (Fig. 2). Notably, compared with the s-MCI group, c-MCI subjects showed atrophy in the left hippocampal tail and subiculum (body) and right subiculum (head) (Table 4). Moreover, this group showed atrophy of the accessory basal nucleus, the

Table 3
Volumetric analysis of the subcortical structures.

Structure volume/eTIV[a]	HC		s-MCI		c-MCI		AD		ANCOVAs		s-MCI vs. c-MCI
	Mean	SD	Mean	SD	Mean	SD	Mean	SD	$F_{3.232}$	P	
L-Cerebellum	34.9	3.07	33.8	4.51	34.9	4.6	33.8	4.29	1.097	0.351	NA
L-Thalamus	4.41	0.41	4.37	0.62	4.12	0.39	4.03	0.50	10.131	**<0.001**	0.253
L-Caudate	2.23	0.31	2.13	0.30	2.19	0.35	2.15	0.35	1.314	0.271	NA
L-Putamen	2.87	0.35	2.94	0.52	2.81	0.42	2.58	0.50	6.792	**<0.001** <0.001	0.761
L-Pallidum	1.29	0.15	1.20	0.15	1.26	0.16	1.23	0.20	1.400	0.244	NA
L-HP	2.53	0.26	2.46	0.54	2.14	0.28	1.94	0.35	40.664	**<0.001**	**0.004**
L-Amygdala	0.99	0.13	0.89	0.21	0.84	0.15	0.73	0.20	29.813	**<0.001**	0.655
L-Accumbens	0.27	0.07	0.26	0.08	0.23	0.06	0.20	0.06	11.631	**<0.001**	0.453
R-Cerebellum	35.2	3.24	34.8	46.2	35.7	4.09	34.0	4.19	2.051	0.108	NA
R-Thalamus	4.37	0.46	4.30	0.62	4.10	0.38	4.03	0.51	6.575	**<0.001** <0.001	0.501
R-Caudate	2.28	0.32	2.20	0.30	2.28	0.31	2.25	0.38	0.496	0.685	NA
R-Putamen	2.88	0.37	2.91	0.61	2.84	0.42	2.67	0.47	3.255	**0.023**	0.943
R-Pallidum	1.24	0.14	1.19	0.15	1.22	0.17	1.20	0.17	1.093	0.353	NA
R–HP	2.62	0.29	2.50	0.36	2.23	0.34	2.06	0.39	28.336	**<0.001** <0.001	**0.046**
R-Amygdala	1.13	0.15	1.05	0.27	0.92	0.18	0.89	0.20	21.867	**<0.001** <0.001	0.053
R-Accumbens	0.31	0.06	0.28	0.08	0.28	0.05	0.24	0.05	13.483	**<0.001** <0.001	0.969

Abbreviations: AD = Alzheimer's Disease; c = converter; Healthy Control (HC); HP = hippocampus; L = left; MCI = Mild Cognitive Impairment; NA=Not applicable; R = right; s = stable.

[a] values x 10^{-3} are expressed as the mean ± standard deviation (SD). MANCOVA's outputs: F = 3.761, <0.001. Bold values are statistically significant comparisons.

Table 4

Volumetric analysis of the hippocampal subfields.

Volume/eTIV[a]	HC		s-MCI		c-MCI		AD		ANCOVAs		s-MCI vs. c-MCI
	Mean	SD	Mean	SD	Mean	SD	Mean	SD	$F_{3,193}$	P	
L-Hippocampal tail	34.3	4.86	33.2	8.70	28.9	5.93	26.3	5.92	5.059	**0.026**	**0.049**
L-Subiculum body	15.4	1.99	14.6	2.89	12.7	2.50	11.5	2.83	24.605	**<0.001**	**0.050**
L-CA1 body	7.78	1.37	7.29	2.19	6.41	1.61	6.41	1.85	30.878	**<0.001**	0.267
L-Subiculum head	12.2	1.37	11.4	2.97	1.2	2.54	9.13	2.78	10.507	**<0.001**	0.338
L-HP fissure	1.07	1.93	1.10	2.53	1.06	2.11	9.71	2.74	21.122	**<0.001**	NA
L-Presub head	9.19	1.04	8.67	2.23	7.70	1.61	6.79	1.98	3.316	**0.021**	0.185
L-CA1 head	32.9	3.59	31.0	7.03	28.3	6.58	25.9	7.46	27.346	**<0.001**	0.432
L-Presub body	11.0	1.85	1.5	2.69	9.21	1.94	8.32	2.29	17.236	**<0.001**	0.128
L-Parasubiculum	4.69	1.08	4.37	0.97	4.34	1.41	3.98	1.42	19.673	**<0.001**	1.000
L-ML HP head	2.08	2.18	19.5	4.69	17.6	3.85	15.7	4.40	4.514	**0.004**	0.284
L-ML HP body	13.9	1.65	13.1	3.28	11.4	2.17	1.5	2.67	24.959	**<0.001**	0.062
L-GC + ML + DG head	9.49	1.39	8.98	2.07	8.14	1.87	7.29	2.14	27.634	**<0.001**	0.387
L-CA3 body	5.59	1.06	5.28	1.49	4.71	0.97	4.37	1.25	18.787	**<0.001**	0.321
L-GC + ML + DG body	8.23	1.08	7.73	1.79	6.91	1.22	6.22	1.57	13.615	**<0.001**	0.158
L-CA4 head	8.03	1.12	7.63	1.71	6.99	1.48	6.27	1.82	25.438	**<0.001**	0.463
L-CA4 body	7.43	0.95	7.03	1.62	6.31	1.05	5.69	1.42	17.273	**<0.001**	0.186
L-Fimbria	4.50	1.46	3.72	1.30	3.46	1.52	2.80	1.56	23.248	**<0.001**	0.927
L-CA3 head	7.63	1.26	7.30	1.64	6.74	1.62	5.90	1.86	16.727	**<0.001**	0.610
L-HATA	3.84	0.59	3.58	0.83	3.06	0.76	2.85	1.05	14.660	**<0.001**	0.141
R-Hippocampal tail	36.7	4.47	34.8	9.57	31.3	7.18	29.0	6.35	17.744	**<0.001**	0.190
R-Subiculum body	15.3	1.78	14.6	3.56	12.8	2.95	11.6	2.75	17.563	**<0.001**	0.064
R-CA1 body	8.52	1.49	8.28	2.11	7.48	1.74	7.02	1.79	25.634	**<0.001**	0.358
R-Subiculum head	12.0	1.72	11.5	3.33	9.76	2.45	8.94	2.36	9.935	**<0.001**	**0.043**
R–HP fissure	11.6	2.00	11.7	2.98	11.6	2.87	1.6	2.82	21.525	**<0.001**	1.000
R-Presub head	8.81	1.19	8.18	2.07	7.34	1.77	6.45	1.60	2.206	0.088	NA
R-CA1 head	34.2	4.02	33.1	7.85	29.6	7.72	27.2	7.25	28.069	**<0.001**	0.227
R-Presub body	9.94	1.61	9.52	2.33	8.49	1.99	7.79	1.81	14.765	**<0.001**	0.196
R-Parasubiculum	4.45	0.99	4.06	1.19	3.99	1.29	3.70	1.20	16.529	**<0.001**	0.997
R-ML HP head	21.3	2.34	2.5	5.08	18.1	4.20	16.3	4.15	5.952	**0.001**	0.116
R-ML HP body	14.4	1.75	13.7	3.45	12.2	2.42	11.0	2.52	22.359	**<0.001**	0.096
R-GC + ML + DG head	1.1	1.30	9.73	2.37	8.78	2.12	8.04	2.15	24.599	**<0.001**	0.296
R-CA3 body	6.41	1.07	6.01	1.42	5.62	1.15	4.98	1.28	14.391	**<0.001**	0.664
R-GC + ML + DG body	8.53	1.11	8.09	2.09	7.29	1.44	6.66	1.57	15.739	**<0.001**	0.224
R-CA4 head	8.53	0.10	8.23	1.92	7.52	1.74	6.94	1.85	18.515	**<0.001**	0.396
R-CA4 body	7.73	1.05	7.30	1.81	6.63	1.17	6.13	1.46	12.901	**<0.001**	0.286
R-Fimbria	4.09	1.15	3.42	1.38	2.92	1.03	2.67	1.43	16.314	**<0.001**	0.525
R-CA3 head	8.48	1.28	8.15	2.07	7.39	1.89	6.77	2.01	19.233	**<0.001**	0.434
R-HATA	4.02	0.70	3.76	1.04	3.22	1.06	3.06	1.03	12.537	**<0.001**	0.168

Abbreviations: AD = Alzheimer's Disease; c = converter; GC + ML + DG = Granule Cell + Molecular Layer + Dentate Gyrus; HC=Healthy Control; HATA=Hippocampal-Amygdaloid Transition Area; HP = hippocampus; L = left; MCI = Mild Cognitive Impairment; ML = molecular layer; NA=Not applicable; Presub = Presubiculum; R = right; s = stable.

[a] values x 10^{-4} are expressed as the mean ± standard deviation (SD). MANCOVA's outputs: F = 1,861, p=<0.001. Bold values are statistically significant comparisons.

central nucleus, and the cortical nucleus of the right amygdala (Table 5). Demographic factors did not significantly influence subregion atrophy in the hippocampus subfields (Supplementary Table 8), whereas the differences in the amygdala nuclei are only influenced by sex (Supplementary Table 10). However, MANCOVA analysis has been restricted to MCI subsets, effects of sex on group differences are no longer significant. Therefore, sex per se does not influence the differences we observe between s-MCI vs c-MCI groups. No significant correlation was found between the MRI volumes and the longitudinal variation of neuropsychological/clinical test scores in the c-MCI group (Supplementary Table 11).

3.4. Stepwise linear discriminant analysis and ROC curves

The stepwise LDA identified a linear combination of predictors that maximized the separation between MCI groups (Fig. 3). The cross-validated AUC was 0.77 (p = $3 \bullet 10^{-4}$) with a best cut-off value sensitivity of 0.78 and a specificity of 0.62. The AUC of the model was higher than the AUCs calculated for each hippocampal and amygdala subregion (Supplementary Table 12) or for the whole hippocampal structure (AUCs: left = 0.73; right = 0.70). The number of predictors selected was always 3 for each cross-validated iteration. The most selected group of regions was the hippocampus's left subiculum (body, selected for all iterations), the left paralaminar nucleus (selected for 34 iterations out of 52), and the right basal nucleus (selected for 30 iterations). Frequent additional selections were the left lateral nucleus and the right accessory basal nucleus (both selected 18 times).

Table 5
Volumetric analysis of the amygdala nuclei.

Volume nucleus/eTIV[a]	HC		s-MCI		c-MCI		AD		ANCOVAs		c-MCI vs s-MCI
	Mean	SD	Mean	SD	Mean	SD	Mean	SD	$F_{3,193}$	P	
L-Lateral	42.8	4.30	38.6	8.11	38.0	7.87	34.5	9.96	16.390	**<0.001**	0.994
L-Basal	28.5	2.92	25.9	5.48	24.4	5.65	21.9	6.44	23.028	**<0.001**	0.731
L-Accessory Basal	16.0	1.84	14.6	3.44	12.9	3.09	11.3	3.52	34.508	**<0.001**	0.163
L-AAA	3.44	0.54	3.13	0.75	2.96	0.68	2.76	0.76	13.691	**<0.001**	0.820
L-Central	2.87	0.62	2.53	0.60	2.17	0.69	1.90	0.68	30.944	**<0.001**	0.224
L-Medial	1.31	0.45	1.20	0.37	1.07	0.46	0.97	0.37	9.455	**<0.001**	0.705
L-Cortical	1.48	0.34	1.40	0.36	1.22	0.37	1.07	0.34	19.302	**<0.001**	0.275
L-CATA	11.0	1.32	1.0	2.11	9.36	2.19	8.54	2.60	18.171	**<0.001**	0.698
L-Paralaminar	3.37	0.40	3.06	0.56	3.02	0.70	2.74	0.81	13.139	**<0.001**	0.998
R-Lateral	43.7	4.63	4.3	8.08	37.1	8.78	35.4	9.52	16.298	**<0.001**	0.478
R-Basal	29.4	3.54	27.6	5.59	24.6	6.32	22.5	6.27	22.154	**<0.001**	0.229
R-Accessory Basal	17.0	2.24	15.9	3.90	13.5	3.61	12.1	3.35	32.916	**<0.001**	**0.032**
R-AAA	3.62	5.62	3.49	0.72	3.12	0.75	2.84	0.77	18.064	**<0.001**	0.234
R-Central	3.06	0.63	2.93	1.01	2.38	0.80	2.16	0.71	20.867	**<0.001**	**0.038**
R-Medial	1.46	0.44	1.36	0.47	1.17	0.42	1.18	0.42	6.371	0.001	0.425
R-Cortical	1.66	0.30	1.54	0.38	1.28	0.38	1.21	0.31	27.310	**<0.001**	**0.026**
R-CATA	11.3	1.48	1.6	2.34	9.37	2.23	8.79	2.31	19.933	**<0.001**	0.180
R-Paralaminar	3.39	0.40	3.14	0.53	2.91	0.75	2.74	0.78	13.375	**<0.001**	0.589

Abbreviations: AAA = Anterior Amygdaloid Area; AD = Alzheimer's Disease; CATA=Cortical-Amygdaloid Transition Area; c-MCI = patients with MCI who convert to AD within 48-month follow-up; HC = healthy control stable after 48 months of follow-up; L = left; R = right; s-MCI = patients with MCI who remain stable within the 48-month follow-up.

[a] values x 10^{-5} are expressed as the mean ± standard deviation (SD). MANCOVA's outputs: F = 3.192, p=<0.001. Bold values are statistically significant comparisons.
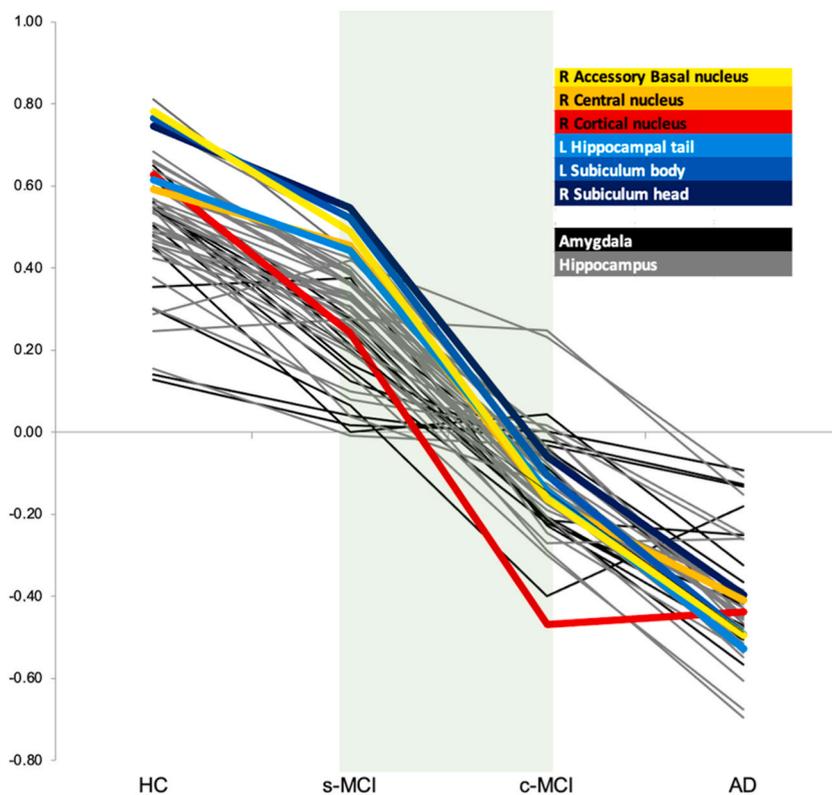
Fig. 2. Line plots illustrating the average distribution of subregions volumes based on the clinical status of participants (HC, s-MCI, c-MCI, and AD). The bold color lines indicated subregions where atrophy was more pronounced in the c-MCI group compared to the s-MCI group. On the other hand, grey and black lines were used for subregions that did not show significant differences in atrophy between the c-MCI and s-MCI groups.
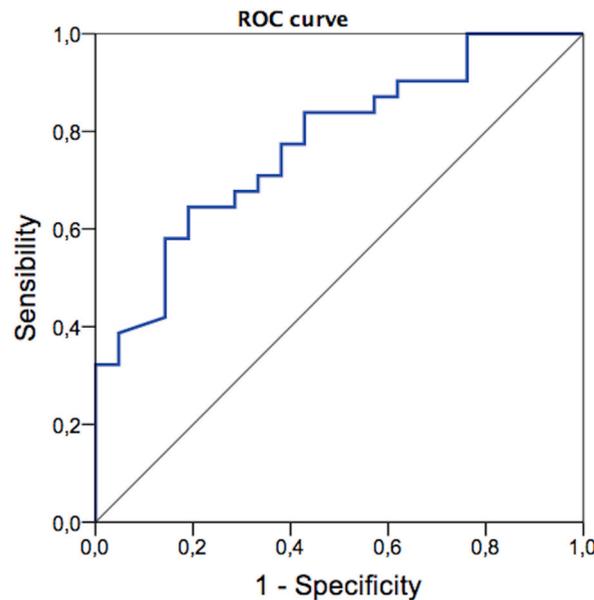
Fig. 3. Receiver Operating Characteristic (ROC) curve of the obtained model.

4. Discussion

The primary aim of the present study was to characterize the morphometric changes of specific subregions of the hippocampus and amygdala in patients suffering from the MCI-AD spectrum. Whereas AD individuals showed widespread atrophy of the hippocampus and amygdala subcortical structures, the progression from MCI to AD involved a more restricted number of subregions. These included the hippocampus's subiculum and tail and the amygdala's accessory basal nucleus, central nucleus, and cortical nucleus. As expected, no significant macrostructural alterations were observed when comparing s-MCI and HC subjects. A discriminant function identified a combination of subregions that maximizes the accurate classification of MCI subjects progressing to AD within 48 months from baseline evaluations (c-MCI). The analysis confirmed the critical role of the hippocampal subiculum (body) in differentiating the c-MCI and s-MCI subsets.

In agreement with previous MRI studies on MCI subjects [16,45], our findings indicate a significant association between whole hippocampal atrophy and MCI progression to AD. However, while hippocampal atrophy can reflect general structural changes, it may not capture the specific underlying pathophysiological processes involved in AD and its clinical progression. Therefore, in the present study, we adopted a more analytic approach, investigating the specific hippocampal subfields that show the earliest and most robust signs of undergoing neurodegeneration. Our results indicate that the atrophy of the subiculum is particularly relevant in the conversion from MCI to AD. This is consistent with histological studies showing a hierarchical progression of tau deposition along the hippocampus [33]. In particular, hippocampal input regions and projection zones (such as the lateral entorhinal cortex, the CA1/subiculum border, and the outer molecular layer of the dentate gyrus) are initially affected by AD pathology. The process develops with anterograde progression through the hippocampal circuitry [46–49]. Our results are also consistent with the results of seminal studies that have investigated the spatial selectivity of hippocampal atrophy in a small sample of MCI individuals with a coarse spatial resolution [12,17,50–52]. In the present study, we leveraged the size of the ADNI database to obtain a systematic follow-up on a well-characterized group of subjects across the AD spectrum. We confirmed the importance of the atrophy of the subiculum in a large subject sample with finer spatial resolutions.

Contrary to our hypothesis, we did not find higher atrophy of the CA1 hippocampal fields in c-MCI compared to s-MCI individuals. However, we did observe a significant CA1 atrophy when comparing c-MCI and AD subjects versus the control group, suggesting the involvement of this region in the clinical, rather than prodromal, AD stage. We also observed atrophy of the hippocampal tail in c-MCI subjects compared to s-MCI individuals. This finding is not commonly reported in AD and could be attributed to the suboptimal sensitivity of previous studies. Thus, the result requires confirmation by future studies. We propose that the atrophy of the hippocampal tail may be explained by the increased vulnerability of this structure to Aβ accumulation occurring in the early stages of AD. This notion is supported by the results of a preclinical study that found smaller hippocampal tail volumes in individuals with the Aβ+ status [53]. These findings highlight the complex and multifaceted nature of hippocampal alterations in AD and the importance of studying specific subfields.

It is important to note that the overall volume of the amygdala did not differ significantly between c-MCI and s-MCI individuals, again suggesting the suboptimal sensitivity of analyses that consider subcortical structures as a whole. When examining the atrophy of specific amygdala nuclei, three nuclei - the accessory basal nucleus, the central nucleus, and the cortical nucleus - showed significant atrophy in c-MCI compared to s-MCI individuals. These findings align with previous data showing the presence of neurofibrillary

tangles and neuritic plaques in the accessory basal and cortical nuclei, while the medial and lateral nuclei appeared relatively spared [32]. The central nucleus, which is known to be affected by the accumulation of neurofibrillary tangles and Aβ [20,54–56], may contribute to the propagation of pathology through a "prion-like" mechanism [20]. Additionally, the central nucleus has important connections with modulatory circuits, including the basal forebrain cholinergic system [57], a region disrupted in AD [58].

The current study has several strengths that contribute to its robustness and reliability. Firstly, the use of the substantial sample obtained from the ADNI-3 database allowed us to adopt stringent screening criteria and a 4-year clinical follow-up, ensuring the accuracy of the diagnosis in the HC and s-MCI groups. Second, the integration of a LDA and ROC analyses provides notable advantages. The discriminant function analysis identifies a linear combination of predictors that maximizes the separation between stable and AD-converter MCI individuals. Moreover, cross-validation provides a more accurate and reliable assessment of the model's performance, reducing the risk of overfitting and supporting the selection of an optimal model. On the other hand, the ROC analysis allows for a comprehensive assessment of classification performance by plotting the trade-off between sensitivity (true positive rate) and specificity (true negative rate), providing a robust measure of diagnostic accuracy.

However, the study also has some limitations that need to be acknowledged. First, despite the richness of the ADNI-3 database, the sample size used in the present study was relatively small, limiting the generalizability of our results. Moreover, the demographic information of our study does not align with the demographic characteristics observed in other previous studies across the AD spectrum, especially concerning the variable of sex [59–61], which, in some cases, also influences the trend of our results. This discrepancy is likely due to the stringent inclusion criteria, such as the selective inclusion of subjects with complete information at baseline and 48 months, that we deliberately chose to ensure the accuracy of our findings. Third, the cross-sectional design does not allow for capturing longitudinal changes in brain atrophy, which could provide valuable information for predicting the progression to more advanced stages of the disease. Including longitudinal MRI analyses with more powerful scanners (e.g., 7 T) would offer a more comprehensive understanding of the timing, spatial distribution, and progression of hippocampal and amygdala involvement in AD. Fourth, alternative methodological approaches should be considered to investigate the patterns that emerged from this study. Advancements in imaging techniques, such as diffusion tensor imaging and molecular imaging using tau and amyloid PET can also provide insights into the morphological and functional alterations associated with MCI and AD [62,63]. It is also important to note that we did not find significant associations between cognitive tests and measures of atrophy of specific subregions despite the well-established involvement of these structures in cognitive functions, such as long-term memory. This negative finding could be explained by the high educational levels of the participants, which may act as a compensatory mechanism between structural alterations and clinical outcomes. Theoretical models have proposed that individuals with higher cognitive reserve can access greater cognitive resources to compensate for cognitive decline [64]. Future studies employing more sensitive assessment protocols and including comprehensive cognitive evaluations may help to detect subtle changes in cognitive and behavioral functioning over time.

4.1. Conclusions

Our findings highlight the importance of performing targeted assessments within the intricate structures of the amygdala and hippocampus to improve early detection of AD progression. The investigation of longitudinal changes in these regions and the use of advanced multimodal MRI techniques are emerging as crucial steps.

Ethical standards

The study was approved by the ethics committees of all participating ADNI sites. Participants or surrogates provide informed consent before participation. All procedures were performed in accordance with the ethical standards laid down in the Declaration of Helsinki and its later amendments.

Funding

CRediT authorship contribution statement

Miriam Punzi: Writing – original draft, Formal analysis, Data curation. **Carlo Sestieri:** Writing – original draft, Methodology, Investigation, Conceptualization. **Eleonora Picerni:** Writing – review & editing. **Antonio Maria Chiarelli:** Writing – review & editing, Methodology, Formal analysis. **Caterina Padulo:** Writing – review & editing. **Andrea Delli Pizzi:** Writing – review & editing. **Maria Giulia Tullo:** Writing – review & editing. **Annalisa Tosoni:** Writing – review & editing. **Alberto Granzotto:** Writing – review & editing. **Stefania Della Penna:** Writing – review & editing. **Marco Onofrj:** Writing – review & editing. **Antonio Ferretti:** Writing – review & editing. **Stefano Delli Pizzi:** Writing – original draft, Supervision, Methodology, Investigation, Funding acquisition, Formal analysis, Data curation, Conceptualization. **Stefano L. Sensi:** Writing – original draft, Supervision, Methodology, Investigation.

Declaration of competing interest

The authors declare that they have no known competing financial interests or personal relationships that could have appeared to influence the work reported in this paper.

Acknowledgements

Appendix A. Supplementary data

Supplementary data to this article can be found online at https://doi.org/10.1016/j.heliyon.2024.e27429.

References

[1] Alzheimer's Disease Facts and Figures, Alzheimers Dement, 2023, https://doi.org/10.1002/alz.13016. Epub ahead of print. PMID: 36918389.

[2] N.D. Anderson, State of the science on mild cognitive impairment (MCI), CNS Spectr. 24 (1) (2019) 78–87, https://doi.org/10.1017/S1092852918001347.

[3] C.R. Jack Jr., D.S. Knopman, W.J. Jagust, R.C. Petersen, M.W. Weiner, P.S. Aisen, L.M. Shaw, P. Vemuri, H.J. Wiste, S.D. Weigand, T.G. Lesnick, V.S. Pankratz, M.C. Donohue, J.Q. Trojanowski, Tracking pathophysiological processes in Alzheimer's disease: an updated hypothetical model of dynamic biomarkers, Lancet Neurol. 12 (2) (2013) 207–216, https://doi.org/10.1016/S1474-4422(12)70291-0.

[4] D. Ciavardelli, F. Piras, A. Consalvo, C. Rossi, M. Zucchelli, C. Di Ilio, V. Frazzini, C. Caltagirone, G. Spalletta, S.L. Sensi, Medium-chain plasma acylcarnitines, ketone levels, cognition, and gray matter volumes in healthy elderly, mildly cognitively impaired, or Alzheimer's disease subjects, Neurobiol. Aging 43 (2016) 1–12, https://doi.org/10.1016/j.neurobiolaging.2016.03.005. Epub 2016 Mar 15. PMID: 27255810.

[5] S. Delli Pizzi, M. Punzi, S.L. Sensi, Alzheimer's Disease Neuroimaging Initiative, Alzheimer's Disease Neuroimaging Initiative. Functional signature of conversion of patients with mild cognitive impairment, Neurobiol. Aging 74 (2019) 21–37, https://doi.org/10.1016/j.neurobiolaging.2018.10.004.

[6] H. Zhang, Z. Wang, K.H. Chan, Y.F. Shea, C.Y. Lee, P.K. Chiu, P. Cao, H.K. Mak, The Use of diffusion Kurtosis imaging for the differential diagnosis of Alzheimer's disease spectrum, Brain Sci. 13 (4) (2023) 595, https://doi.org/10.3390/brainsci13040595.

[7] K. Kwak, M. Niethammer, K.S. Giovanello, M. Styner, E. Dayan, Alzheimer's Disease Neuroimaging Initiative, Differential role for hippocampal subfields in Alzheimer's disease progression revealed with deep learning, Cerebr. Cortex 32 (3) (2022) 467–478, https://doi.org/10.1093/cercor/bhab223.

[8] S. Guo, B. Xiao, C. Wu, Alzheimer's Disease Neuroimaging Initiative, Identifying subtypes of mild cognitive impairment from healthy aging based on multiple cortical features combined with volumetric measurements of the hippocampal subfields, Quant. Imag. Med. Surg. 10 (7) (2020) 1477–1489, https://doi.org/10.21037/qims-19-872.

[9] J. Izzo, O.A. Andreassen, L.T. Westlye, D. van der Meer, The association between hippocampal subfield volumes in mild cognitive impairment and conversion to Alzheimer's disease, Brain Res. 1728 (2020) 146591, https://doi.org/10.1016/j.brainres.2019.146591.

[10] R. Vasta, A. Augimeri, A. Cerasa, S. Nigro, V. Gramigna, M. Nonnis, F. Rocca, G. Zito, A. Quattrone, For The Alzheimer's Disease Neuroimaging Initiative, Hippocampal subfield Atrophies in converted and not-converted mild cognitive impairments patients by a markov random fields algorithm, Curr. Alzheimer Res. 13 (5) (2016) 566–574, https://doi.org/10.2174/1567205013666160120151457.

[11] W. Khan, E. Westman, N. Jones, L.O. Wahlund, P. Mecocci, B. Vellas, M. Tsolaki, I. Kłoszewska, H. Soininen, C. Spenger, S. Lovestone, J.S. Muehlboeck, A. Simmons, AddNeuroMed consortium and for the Alzheimer's Disease Neuroimaging Initiative, Automated hippocampal subfield measures as predictors of conversion from mild cognitive impairment to Alzheimer's disease in two independent cohorts, Brain Topogr. 28 (5) (2015) 746–759, https://doi.org/10.1007/s10548-014-0415-1.

[12] L.G. Apostolova, R.A. Dutton, I.D. Dinov, K.M. Hayashi, A.W. Toga, J.L. Cummings, P.M. Thompson, Conversion of mild cognitive impairment to Alzheimer's disease predicted by hippocampal atrophy maps, Arch. Neurol. 63 (5) (2006) 693–699, https://doi.org/10.1001/archneur.63.5.693.

[13] L.G. Apostolova, L. Mosconi, P.M. Thompson, A.E. Green, K.S. Hwang, A. Ramirez, R. Mistur, W.H. Tsui, M.J. de Leon, Subregional hippocampal atrophy predicts Alzheimer's dementia in the cognitively normal, Neurobiol. Aging 31 (7) (2010) 1077–1088, https://doi.org/10.1016/j.neurobiolaging.2008.08.008.

[14] C.R. Jack Jr., R.C. Petersen, Y. Xu, P.C. O'Brien, G.E. Smith, R.J. Ivnik, B.F. Boeve, E.G. Tangalos, E. Kokmen, Rates of hippocampal atrophy correlate with change in clinical status in aging and AD, Neurology 55 (4) (2000) 484–489, https://doi.org/10.1212/wnl.55.4.484.

[15] R. Duara, D.A. Loewenstein, E. Potter, J. Appel, M.T. Greig, R. Urs, Q. Shen, A. Raj, B. Small, W. Barker, E. Schofield, Y. Wu, H. Potter, Medial temporal lobe atrophy on MRI scans and the diagnosis of Alzheimer's disease, Neurology 71 (24) (2008) 1986–1992, https://doi.org/10.1212/01.wnl.0000336925.79704.9f.

[16] S.L. Risacher, A.J. Saykin, J.D. West, L. Shen, H.A. Firpi, B.C. McDonald, Alzheimer's Disease Neuroimaging Initiative (ADNI), Baseline MRI predictors of conversion from MCI to probable AD in the ADNI cohort, Curr. Alzheimer Res. 6 (4) (2009) 347–361, https://doi.org/10.2174/156720509788929273.

[17] D.P. Devanand, R. Bansal, J. Liu, X. Hao, G. Pradhaban, B.S. Peterson, MRI hippocampal and entorhinal cortex mapping in predicting conversion to Alzheimer's disease, Neuroimage 60 (3) (2012) 1622–1629, https://doi.org/10.1016/j.neuroimage.2012.01.075.

[18] G. Halliday, Pathology and hippocampal atrophy in Alzheimer's disease, Lancet Neurol. 16 (11) (2017) 862–864, https://doi.org/10.1016/S1474-4422(17)30343-5.

[19] H. Braak, K. Del Tredici, The preclinical phase of the pathological process underlying sporadic Alzheimer's disease, Brain 138 (Pt 10) (2015) 2814–2833, https://doi.org/10.1093/brain/awv236.

[20] P.T. Nelson, E.L. Abner, E. Patel, S. Anderson, D.M. Wilcock, R.J. Kryscio, L.J. Van Eldik, G.A. Jicha, Z. Gal, R.S. Nelson, B.G. Nelson, J. Gal, M.T. Azam, D. W. Fardo, M.D. Cykowski, The amygdala as a locus of pathologic misfolding in neurodegenerative diseases, J. Neuropathol. Exp. Neurol. 77 (1) (2018) 2–20, https://doi.org/10.1093/jnen/nlx099.

[21] K.M. Stouffer, C. Chen, S. Kulason, E. Xu, M.P. Witter, C. Ceritoglu, M.S. Albert, S. Mori, J. Troncoso, D.J. Tward, M.I. Miller, Alzheimer's Disease Neuroimaging Initiative, Early amygdala and ERC atrophy linked to 3D reconstruction of rostral neurofibrillary tau tangle pathology in Alzheimer's disease, Neuroimage Clin 38 (2023) 103374, https://doi.org/10.1016/j.nicl.2023.103374.

[22] H. Hampel, S. Lista, Dementia: the rising global tide of cognitive impairment, Nat. Rev. Neurol. 12 (3) (2016) 131–132, https://doi.org/10.1038/nrneurol.2015.250.

[23] A. Bejanin, D.R. Schonhaut, R. La Joie, J.H. Kramer, S.L. Baker, N. Sosa, N. Ayakta, A. Cantwell, M. Janabi, M. Lauriola, J.P. O'Neil, M.L. Gorno-Tempini, Z. A. Miller, H.J. Rosen, B.L. Miller, W.J. Jagust, G.D. Rabinovici, Tau pathology and neurodegeneration contribute to cognitive impairment in Alzheimer's disease, Brain 140 (12) (2017) 3286–3300, https://doi.org/10.1093/brain/awx243.

[24] M.A. Busche, S. Wegmann, S. Dujardin, C. Commins, J. Schiantarelli, N. Klickstein, T.V. Kamath, G.A. Carlson, I. Nelken, B.T. Hyman, Tau impairs neural circuits, dominating amyloid-β effects, in Alzheimer models in vivo, Nat. Neurosci. 22 (1) (2019) 57–64, https://doi.org/10.1038/s41593-018-0289-8.

[25] O. Abiose, K.D. Deters, C. Young, E.C. Mormino, Amygdala tau in preclinical Alzheimer's disease: neuroimaging/normal brain aging, Alzheimers Dement 16 (2020) e046762, https://doi.org/10.1002/alz.046762.2023.

[26] D. Berron, J.W. Vogel, P.S. Insel, J.B. Pereira, L. Xie, L.E.M. Wisse, P.A. Yushkevich, S. Palmqvist, N. Mattsson-Carlgren, E. Stomrud, R. Smith, O. Strandberg, O. Hansson, Early stages of tau pathology and its associations with functional connectivity, atrophy and memory, Brain 144 (9) (2021) 2771–2783, https://doi.org/10.1093/brain/awab114.

[27] J.W. Vogel, A.L. Young, N.P. Oxtoby, R. Smith, R. Ossenkoppele, O.T. Strandberg, R. La Joie, L.M. Aksman, M.J. Grothe, Y. Iturria-Medina, Alzheimer's Disease Neuroimaging Initiative, M.J. Pontecorvo, M.D. Devous, G.D. Rabinovici, D.C. Alexander, C.H. Lyoo, A.C. Evans, O. Hansson, Four distinct trajectories of tau deposition identified in Alzheimer's disease, Nat. Med. 27 (5) (2021) 871–881, https://doi.org/10.1038/s41591-021-01309-6.

[28] Z.M. Saygin, D. Kliemann, J.E. Iglesias, A.J.W. van der Kouwe, E. Boyd, M. Reuter, A. Stevens, K. Van Leemput, A. McKee, M.P. Frosch, B. Fischl, J. C. Augustinack, Alzheimer's Disease Neuroimaging Initiative, High-resolution magnetic resonance imaging reveals nuclei of the human amygdala: manual segmentation to automatic atlas, Neuroimage 155 (2017) 370–382, https://doi.org/10.1016/j.neuroimage.2017.04.046.

[29] G. Simić, I. Kostović, B. Winblad, N. Bogdanović, Volume and number of neurons of the human hippocampal formation in normal aging and Alzheimer's disease, J. Comp. Neurol. 379 (1997) 482–494, https://doi.org/10.1002/(sici)1096-9861(19970324)379:4<482::aid-cne2>3.0.co;2-z.

[30] A.J. Harding, G.M. Halliday, J.J. Kril, Variation in hippocampal neuron number with age and brain volume, Cerebr. Cortex 8 (8) (1998) 710–718, https://doi.org/10.1093/cercor/8.8.710.

[31] K. Amunts, O. Kedo, M. Kindler, P. Pieperhoff, H. Mohlberg, N.J. Shah, U. Habel, F. Schneider, K. Zilles, Cytoarchitectonic mapping of the human amygdala, hippocampal region and entorhinal cortex: intersubject variability and probability maps, Anat. Embryol. 210 (5–6) (2005) 343–352, https://doi.org/10.1007/s00429-005-0025-5.

[32] K.L.J. Vogt, B.T. Hyman, G.W. Van Hoesen, A.R. Damasio, Pathological alterations in the amygdala in Alzheimer's disease, Neuroscience 37 (2) (1990) 377–385, https://doi.org/10.1016/0306-4522(90)90408-v.

[33] L. Zhang, Y. Jiang, J. Zhu, H. Liang, X. He, J. Qian, H. Lin, Y. Tao, K. Zhu, Quantitative assessment of hippocampal tau pathology in AD and PART, J. Mol. Neurosci. 70 (11) (2020) 1808–1811, https://doi.org/10.1007/s12031-020-01573-0.

[34] S.G. Mueller, N. Schuff, K. Yaffe, C. Madison, B. Miller, M.W. Weiner, Hippocampal atrophy patterns in mild cognitive impairment and Alzheimer's disease, Hum. Brain Mapp. 31 (9) (2010) 1339–1347, https://doi.org/10.1002/hbm.20934.

[35] B.J. Hanseeuw, K. Van Leemput, M. Kavec, C. Grandin, X. Seron, A. Ivanoiu, Mild cognitive impairment: differential atrophy in the hippocampal subfields, AJNR Am J Neuroradiol 32 (9) (2011) 1658–1661, https://doi.org/10.3174/ajnr.A2589.

[36] L.E. Wisse, G.J. Biessels, S.M. Heringa, H.J. Kuijf, D.H. Koek, P.R. Luijten, M.I. Geerlings, Utrecht Vascular Cognitive Impairment (VCI) Study Group, Hippocampal subfield volumes at 7T in early Alzheimer's disease and normal aging, Neurobiol. Aging 35 (9) (2014) 2039–2045, https://doi.org/10.1016/j.neurobiolaging.2014.02.021.

[37] G.A. Carlesimo, F. Piras, M.D. Orfei, M. Iorio, C. Caltagirone, G. Spalletta, Atrophy of presubiculum and subiculum is the earliest hippocampal anatomical marker of Alzheimer's disease, Alzheimers Dement (Amst) 1 (1) (2015) 24–32, https://doi.org/10.1016/j.dadm.2014.12.001.

[38] U. Khatri, G.R. Kwon, Alzheimer's disease diagnosis and biomarker analysis using resting-state functional MRI functional brain network with multi-measures features and hippocampal subfield and amygdala volume of structural MRI, Front. Aging Neurosci. 14 (2022) 818871, https://doi.org/10.3389/fnagi.2022.818871.

[39] L. Göschel, L. Kurz, A. Dell'Orco, T. Köbe, P. Körtvélyessy, A. Fillmer, S. Aydin, L.T. Riemann, H. Wang, B. Ittermann, U. Grittner, A. Flöel, 7T amygdala and hippocampus subfields in volumetry-based associations with memory: a 3-year follow-up study of early Alzheimer's disease, Neuroimage Clin 38 (2023) 103439, https://doi.org/10.1016/j.nicl.2023.103439.

[40] H. Qu, H. Ge, L. Wang, W. Wang, C. Hu, Volume changes of hippocampal and amygdala subfields in patients with mild cognitive impairment and Alzheimer's disease, Acta Neurol. Belg. 123 (4) (2023) 1381–1393, https://doi.org/10.1007/s13760-023-02235-9.

[41] J.E. Iglesias, J.C. Augustinack, K. Nguyen, C.M. Player, A. Player, M. Wright, N. Roy, M.P. Frosch, A.C. McKee, L.L. Wald, B. Fischl, K. Van Leemput, Alzheimer's Disease Neuroimaging Initiative, A computational atlas of the hippocampal formation using ex vivo, ultra-high resolution MRI: application to adaptive segmentation of in vivo MRI, Neuroimage 115 (2015) 117–137, https://doi.org/10.1016/j.neuroimage.2015.04.042.

[42] H. Cho, J.H. Kim, C. Kim, B.S. Ye, H.J. Kim, C.W. Yoon, Y. Noh, G.H. Kim, Y.J. Kim, J.H. Kim, C.H. Kim, S.J. Kang, J. Chin, S.T. Kim, K.H. Lee, D.L. Na, J. K. Seong, S.W. Seo, Shape changes of the basal ganglia and thalamus in Alzheimer's disease: a three-year longitudinal study, J Alzheimers Dis 40 (2) (2014) 285–295, https://doi.org/10.3233/JAD-132072.

[43] J.P. Aggleton, A. Pralus, A.J. Nelson, M. Hornberger, Thalamic pathology and memory loss in early Alzheimer's disease: moving the focus from the medial temporal lobe to Papez circuit, Brain 139 (Pt 7) (2016) 1877–1890, https://doi.org/10.1093/brain/aww083.

[44] A.J. Saykin, L. Shen, T.M. Foroud, S.G. Potkin, S. Swaminathan, S. Kim, S.L. Risacher, K. Nho, M.J. Huentelman, D.W. Craig, P.M. Thompson, J.L. Stein, J. H. Moore, L.A. Farrer, R.C. Green, L. Bertram, C.R. Jack Jr., M.W. Weiner, Alzheimer's Disease Neuroimaging Initiative, Alzheimer's Disease Neuroimaging Initiative biomarkers as quantitative phenotypes: genetics core aims, progress, and plans, Alzheimers Dement 6 (3) (2010) 265–273, https://doi.org/10.1016/j.jalz.2010.03.013.

[45] D.P. Devanand, G. Pradhaban, X. Liu, A. Khandji, S. De Santi, S. Segal, H. Rusinek, G.H. Pelton, L.S. Honig, R. Mayeux, Y. Stern, M.H. Tabert, M.J. de Leon, Hippocampal and entorhinal atrophy in mild cognitive impairment: prediction of Alzheimer disease, Neurology 68 (11) (2007) 828–836, https://doi.org/10.1212/01.wnl.0000256697.20968.d7.

[46] H. Braak, E. Braak, Frequency of stages of Alzheimer-related lesions in different age categories, Neurobiol. Aging 18 (4) (1997) 351–357, https://doi.org/10.1016/s0197-4580(97)00056-0.

[47] G. Lace, G.M. Savva, G. Forster, R. de Silva, C. Brayne, F.E. Matthews, J.J. Barclay, L. Dakin, P.G. Ince, S.B. Wharton, Mrc-Cfas, Hippocampal tau pathology is related to neuroanatomical connections: an ageing population-based study, Brain 132 (Pt 5) (2009) 1324–1334, https://doi.org/10.1093/brain/awp059.

[48] L. Liu, V. Drouet, J.W. Wu, M.P. Witter, S.A. Small, C. Clelland, K. Duff, Trans-synaptic spread of tau pathology in vivo, PLoS One 7 (2) (2012) e31302, https://doi.org/10.1371/journal.pone.0031302.

[49] P.A. Yushkevich, M. Muñoz López, M.M. Iñiguez de Onzoño Martin, R. Ittyerah, S. Lim, S. Ravikumar, M.L. Bedard, S. Pickup, W. Liu, J. Wang, L.Y. Hung, J. Lasserve, N. Vergnet, L. Xie, M. Dong, S. Cui, L. McCollum, J.L. Robinson, T. Schuck, R. de Flores, R. Insausti, Three-dimensional mapping of neurofibrillary tangle burden in the human medial temporal lobe, Brain 144 (9) (2021) 2784–2797, https://doi.org/10.1093/brain/awab262.

[50] G. Chételat, M. Fouquet, G. Kalpouzos, I. Denghien, V. De la Sayette, F. Viader, F. Mézenge, B. Landeau, J.C. Baron, F. Eustache, B. Desgranges, Three-dimensional surface mapping of hippocampal atrophy progression from MCI to AD and over normal aging as assessed using voxel-based morphometry, Neuropsychologia 46 (6) (2008) 1721–1731, https://doi.org/10.1016/j.neuropsychologia.2007.11.037.

[51] L. Su, L. Hayes, S. Soteriades, G. Williams, S.A.E. Brain, M.J. Firbank, G. Longoni, R.J. Arnold, J.B. Rowe, J.T. O'Brien, Hippocampal stratum radiatum, lacunosum, and moleculare sparing in mild cognitive impairment, J Alzheimers Dis 61 (1) (2018) 415–424, https://doi.org/10.3233/JAD-170344.

[52] Q. Zeng, K. Li, X. Luo, S. Wang, X. Xu, Z. Li, T. Zhang, X. Liu, Y. Fu, X. Xu, C. Wang, T. Wang, J. Zhou, Z. Liu, Y. Chen, P. Huang, M. Zhang, The Alzheimer's Disease Neuroimaging Initiative, Distinct atrophy pattern of hippocampal subfields in patients with progressive and stable mild cognitive impairment: a longitudinal MRI study, J Alzheimers Dis 79 (1) (2021) 237–247, https://doi.org/10.3233/JAD-200775.

[53] P.J. Hsu, H. Shou, T. Benzinger, D. Marcus, T. Durbin, J.C. Morris, Y.I. Sheline, Amyloid burden in cognitively normal elderly is associated with preferential hippocampal subfield volume loss, J Alzheimers Dis 45 (1) (2015) 27–33, https://doi.org/10.3233/JAD-141743.

[54] K. Tsuchiya, K. Kosaka, Neuropathological study of the amygdala in presenile Alzheimer's disease, J. Neurol. Sci. 100 (1–2) (1990) 165–173, https://doi.org/10.1016/0022-510x(90)90029-m.

[55] H. Braak, E. Braak, Neuropathological stageing of Alzheimer-related changes, Acta Neuropathol. 82 (4) (1991) 239–259, https://doi.org/10.1007/BF00308809.

[56] P.J. Whalen, E.A. Phelps, The Human Amygdala, The Guilford Press, New York, 2009.

[57] J. LeDoux, The amygdala, Curr. Biol. 17 (20) (2007) R868–R874, https://doi.org/10.1016/j.cub.2007.08.005.

[58] H. Hampel, M.M. Mesulam, A.C. Cuello, M.R. Farlow, E. Giacobini, G.T. Grossberg, A.S. Khachaturian, A. Vergallo, E. Cavedo, P.J. Snyder, Z.S. Khachaturian, The cholinergic system in the pathophysiology and treatment of Alzheimer's disease, Brain 141 (7) (2018) 1917–1933, https://doi.org/10.1093/brain/awy132.

[59] D. Sohn, K. Shpanskaya, J.E. Lucas, J.R. Petrella, A.J. Saykin, R.E. Tanzi, N.F. Samatova, P.M. Doraiswamy, Sex differences in cognitive decline in subjects with high likelihood of mild cognitive impairment due to Alzheimer's disease, Sci. Rep. 8 (1) (2018) 7490, https://doi.org/10.1038/s41598-018-25377-w.

[60] D. Zhu, A. Montagne, Z. Zhao, Alzheimer's pathogenic mechanisms and underlying sex difference, Cell. Mol. Life Sci.: CM 78 (11) (2021) 4907–4920, https://doi.org/10.1007/s00018-021-03830-w.

[61] C. Berezuk, M. Khan, B.L. Callahan, J. Ramirez, S.E. Black, K.K. Zakzanis, Alzheimer's Disease Neuroimaging Initiative, Sex differences in risk factors that predict progression from mild cognitive impairment to Alzheimer's dementia, J. Int. Neuropsychol. Soc. : JINS 29 (4) (2023) 360–368, https://doi.org/10.1017/S1355617722000297.

[62] A. Leuzy, K. Chiotis, L. Lemoine, P.G. Gillberg, O. Almkvist, E. Rodriguez-Vieitez, A. Nordberg, Tau PET imaging in neurodegenerative tauopathies-still a challenge, Mol. Psychiatr. 24 (8) (2019) 1112–1134, https://doi.org/10.1038/s41380-018-0342-8.

[63] V.L. Villemagne, V. Doré, S.C. Burnham, C.L. Masters, C.C. Rowe, Imaging tau and amyloid-β proteinopathies in Alzheimer's disease and other conditions, Nat. Rev. Neurol. 14 (4) (2018) 225–236, https://doi.org/10.1038/nrneurol.2018.9.

[64] Y. Stern, Cognitive reserve in ageing and Alzheimer's disease, Lancet Neurol. 11 (11) (2012) 1006–1012, https://doi.org/10.1016/S1474-4422(12)70191-6.